Materials Advances

ROYAL SOCIETY OF CHEMISTRY

PAPER

View Article Online
View Journal | View Issue

Cite this: *Mater. Adv.*, 2022, 3, 8665

Nanocrack-based ultrasensitive wearable and skin-mountable strain sensors for human motion detection

R. Madhavan

Received 11th September 2022,
Accepted 4th October 2022

DOI: 10.1039/d2ma00897a

rsc.li/materials-advances

Advanced wearable and stretchable strain sensing devices for human motion detection are garnering tremendous attention and thus demonstrate substantial potential for future wearable sensors. This work presents network crack-assisted wearable strain sensors using graphite nanoflake spray coated onto highly elastic nitrile elastomers. The as-fabricated wearable strain sensors demonstrate numerous captivating benefits, including simplicity in the construction process and ultra-large strain sensitivity far surpassing the state of art stretchable strain sensors. It is worth mentioning that the stretchable strain sensors possess an ultrasensitive gauge factor (GF) of 868.12 ± 56.90 and a wide sensing range of up to 30% strain. The electromechanical performance depends on the electrical resistance variation, which is substantially altered by percolative microstructural network cracks with strain concentration during mechanical deformations. The ultrasensitive strain monitoring performance in conjunction with a wide sensing range, prominent reversibility, ultrafast response and recovery speeds (7.5 ms, and 5 ms, respectively), and excellent durability (more than 2000 stretching–releasing cycles under a large-scale strain of 30%) enables the strain sensors to be used as electronic skins for wearable monitoring applications, including but not limited to the detection of full-range human activity monitoring, as well as healthcare and biomedical-related vital signs, soft robotics, and entertainment technology.

Introduction

Owing to the rapid development of electronic devices towards high performance and wearability,[1–5,63–65] stretchable and wearable electronic devices capable of multi-scale strain sensing have attracted extensive interest from researchers due to their fascinating applicability in human motion monitoring,[6,7,55–59] personalized healthcare,[8,9] human–machine interaction,[10,11] sport activity monitoring,[12] and soft robotics,[13,14] which have recently caused a tremendous evolution of human lifestyle. The wearable strain sensors on the basis of their transduction mechanisms can be classified as piezoresistive,[15,16] piezocapacitive,[17,18] piezoelectric,[19,20] and optical sensors.[21] Among them, piezoresistive devices, which transduce mechanical deformation into electrical resistance variation, exhibit enormous significance for constructing soft and elastic artificial systems for entire-range human motion/activity monitoring owing to their efficient transduction mechanisms, simple structural designs, low power consumption, and ease of fabrication.[22–25] To this end, wearable sensor networks should demonstrate both high sensitivity and a broad strain range with multi-scale recognition ability.[26–28] To secure high sensitivity in these types of sensing platforms, brittle conductive films are required for substantial structural variation under small-scale mechanical stimulation.[29,30] On the other hand, to accomplish a broad strain sensing range, substantial mechanical resilience is required to maintain the conductive pathways intact even under a large-scale mechanical deformation.[31,32] Therefore, there exists an enormous contradiction between sensitivity and the strain range, which limits the development of an idealized wearable strain sensor.

In recent years, to develop wearable and high performance strain sensors with both high sensitivity and a broad strain sensing range simultaneously, extensive research has been carried out by integrating low-dimensional nanomaterials with elastomeric substrates and textile materials. For instance, Li *et al.* fabricated a high performance nanohybrid strain sensor based on MXene/cellulose nanocrystal (CNC)/thermoplastic polyurethane (TPU) non-woven fabric (NWF) through a dip coating process, which exhibited both high sensitivity (GF ~ 3405) and a broad strain range (up to 83% strain) in a simultaneous fashion.[33] This strain sensor demonstrated an ultrahigh strain sensitivity owing to the variations in the contact area as well as interfacial binding between neighbouring non-woven fabric layers when subjected to dynamic mechanical

Department of Chemical Engineering, Indian Institute of Science, Bengaluru 560012, Karnataka, India. E-mail: madhavan_rajaa@rediffmail.com

deformations. However, the broad strain sensing range of this device was attributed to the higher cellulose nanocrystal (CNC) loading in the electrically conductive sensor network. Liu *et al.* developed a breathable and anti-jamming strain sensor based on copper/viscose yarn fabrics through a polymer-assisted metal deposition process, which demonstrated a high sensitivity (GF $\sim$ 49.5) and a wide sensing range (up to 200% strain) simultaneously.[34] The strain sensitivity of this wearable sensor was attributed to the variation of elastic yarn diameter during the stretching process. Pan *et al.* proposed a sensitivity screenable strain sensor utilizing a new approach of mechanocombinatorics comprising of gold nanofilm/polydimethylsiloxane composites fabricated through a local illumination process with a large strain sensitivity (GF $\sim$ 157).[35] On the other hand, the strain range was limited to 15% strain. The strain sensitivity of this sensor was governed by the strain redistribution over the elastomeric substrates due to its mechanics and structural properties. Niu *et al.* reported a high performance wireless strain sensor based on carbon nanotubes/styrenic thermoplastic elastomers developed by drop-casting functional materials, which demonstrated both high strain sensitivity (GF $\sim$ 201.6) and a wide strain range (up to 50% strain) simultaneously.[36] Kim *et al.* fabricated a high performance multidimensional strain sensor based on Ag nanowire percolation networks through drop-casting, spin-coating, and photolithographic processes.[60] The strain sensor exhibited both a large sensitivity (GF $>$ 20) and a wide sensing range (up to 35% strain) simultaneously. Wang *et al.* developed wearable strain sensing fabrics for real-time sweat volume monitoring.[61] The sensor demonstrated a GF of 2.033 and a strain range of up to 30%. Kim *et al.* reported machine-learning based crack-assisted wearable sensors *via* direct laser writing for human motion/health monitoring.[62] The strain sensor demonstrated an ultrasensitive GF of more than 2000 at 0.55% strain.

Through the consideration of strain sensitivity and sensing range, herein, this work reports a wearable strain sensor with ultra-large strain sensitivity and a broad strain sensing range based on graphite nanoflakes as brittle conductive networks and epidermal-like nitrile elastomers as the stretchable supporting materials. The novel brittle-stretchable conductive network based on graphite material-nitrile elastomers endows the strain sensors with ultra-large strain sensitivity (GF $\sim$ 868.12 $\pm$ 56.90), a broad strain sensing range (up to 30% strain), small hysteresis, super-fast strain response and recovery (7.5 ms, and 5 ms, respectively), and excellent durability (more than 2000 stretch-release cycles under an extensive deformation of 30% strain). Owing to these high performance merits and as a proof of concept, the as-fabricated wearable strain sensors are utilized for full-range detection of human healthcare including monitoring of both minute deformations (facial expressions and larynx muscle movements), and large-strain human motions (human articular joint motions). As compared to the recently reported wearable strain sensors, graphite material-nitrile elastomers exhibit high performance especially an ultra-large strain sensitivity and a broad sensing range. It is envisioned that the as-fabricated wearable devices could offer promising applicability in future wearable electronics.

Experimental section

Materials

The soft, elastic, and skin-like nitrile elastomers were purchased from Rubber House, Ltd. Functional sensor materials based on graphite materials were procured from the Kontakt Chemie, Ltd. For laminating the wearable devices onto the various sensing locations, strong double sided tape was purchased from 3M, Ltd.

Fabrication of the stretchable elastomeric strain sensors

The soft, elastic, and skin-like nitrile elastomers were washed effectively using deionized water (resistivity $\sim$ 18.2 MΩ cm) and ethanol followed by placing firmly onto a rigid support for depositing the functional sensor materials. The graphite based functional sensor materials were spray deposited onto the nitrile elastomers and permitted to dry at room temperature. For conducting electrical-mechanical examinations on the strain sensors, silver wires were connected onto the two ends of the graphite nanoflake conductive film using a fast-drying silver conductive paste (Ted Pella, Inc.)

Characterization

Morphological examination of the graphite nanoflake/nitrile rubber composites at various applied strain levels was carried out using an optical microscope (Inskam, Inc.) The uniform stretching-releasing cyclic strains were applied to the strain sensors using a motorized linear translation stage and the resultant electronic signals were recorded through a digital multimeter (Hantek HDM-3065B). To illustrate the capability of the wearable strain sensors for burgeoning applications in wearable electronics, the wearable devices were laminated onto the human epidermis at various locations by using kinesiology tape for detecting diverse-ranging human bodily motions.

Results and discussion

Fig. 1a illustrates the fabrication process of the as-developed graphite nanoflake/nitrile rubber nanocomposite based strain sensors. The detailed construction procedures are presented in the Experimental section. Fig. 1b demonstrates the prominent stretchability of the as-fabricated wearable and skin-mountable strain sensors. Recently, these wearable devices have been extensively manufactured by embedding or incorporating the active materials on stretchable elastic polymers. In these devices, the micro-structure as well as the electromechanical performance can be easily degraded even by tiny deformation like a human touch.[23,37] On the other hand, the graphite nanoflake/nitrile rubber nanocomposite strain sensors proposed in this work can be mechanically deformed with outstanding stability owing to the prominent adhesion of graphite nanoflake film with the nitrile rubber matrix. Therefore, the graphite nanoflake/nitrile rubber nanocomposites can be effectively mounted onto the human epidermal surface as well as to the complex and irregular objects with negligible degradation to the coating layer. Fig. 1c–e illustrates the top view SEM image and optical cross-section view of

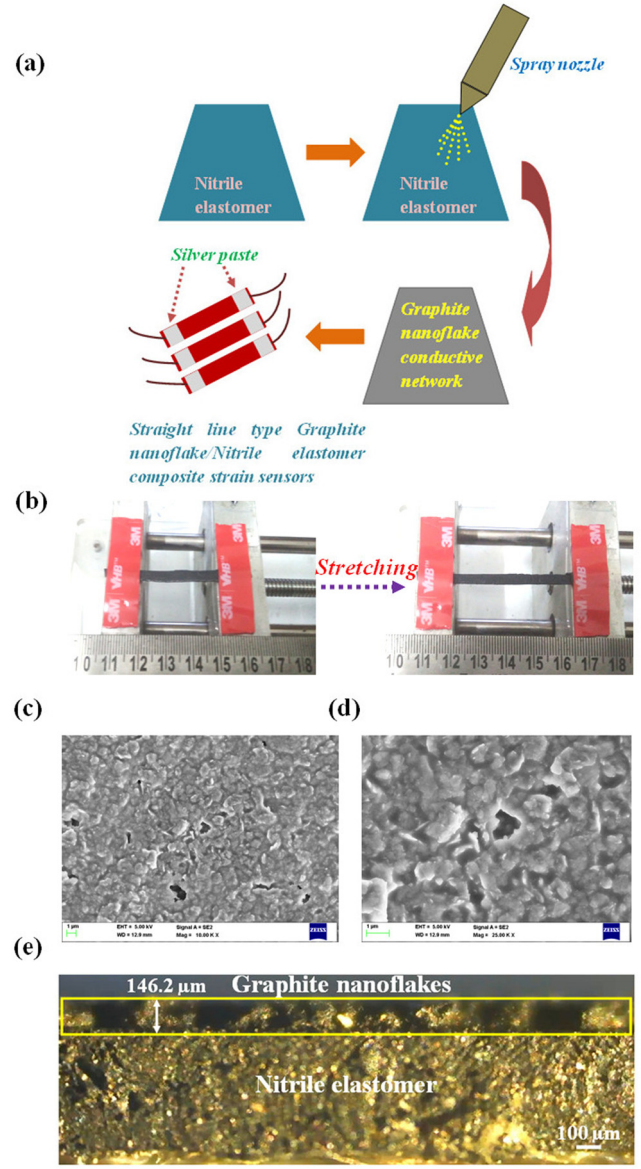

Fig. 1 (a) Scheme of the construction process of the ultrasensitive graphite nanoflake/nitrile elastomer nanocomposite strain sensors. (b) The graphite nanoflake/nitrile elastomer nanocomposite strain sensor demonstrated high stretchability during the application of tensile strains. (c) The SEM image of the graphite nanoflake conductive network. (d) A zoomed-in SEM image of (c). (e) Cross-sectional optical image of graphite nanoflake/nitrile elastomer nanocomposite strain sensors.

the graphite nanoflake/nitrile rubber nanocomposite, indicating the prominent uniformity and excellent adhesion properties. In other words, when the graphite nanoflakes are spray coated onto the surface of nitrile rubber, the interaction of graphite nanoflakes with nitrile rubber chains occurs through van der Waals forces, exhibiting prominent adhesion between the graphite nanoflakes and nitrile rubber. The cross-sectional optical image shows a bilayer network comprised of a conductive layer (graphite nanoflake film) at the top and an elastic stretchable supporting material below it (nitrile elastomer). During the mechanical deformation process, fracture of the conductive network occurred in the graphite nanoflake/nitrile elastomer composite and structural cracks were developed. Furthermore, the conductive network cracks were interconnected with segregated bridge and island structures.

Electromechanical performance

By controlling the shape of the graphite conductive layer embedded onto the nitrile elastomers, strain sensing devices with straight line type design configurations were fabricated with ease. The stretchable strain sensor proposed in this research is designed employing ultra-soft and highly elastic nitrile elastomers which exhibit a tiny weight of just 0.23 g.

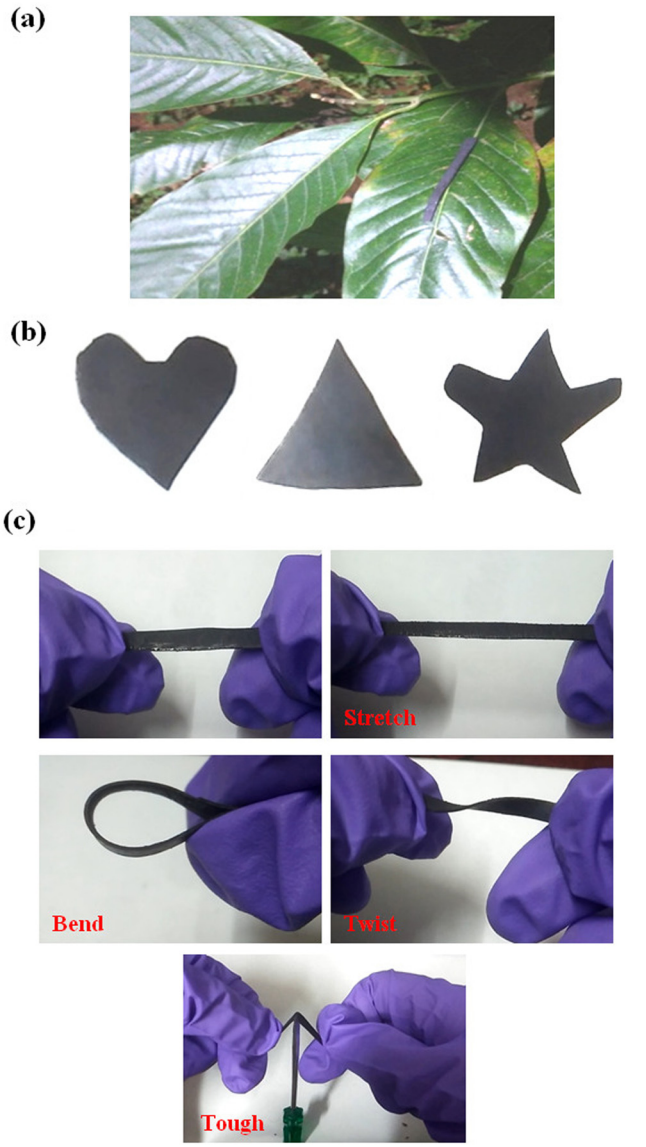

Fig. 2 The robustness and resilience of the graphite nanoflake/nitrile elastomer nanocomposite strain sensors. (a) Graphite nanoflake/nitrile elastomer nanocomposite sensor placed on a leaf to demonstrate its lightweight features. (b) Different shapes of the graphite nanoflake/nitrile elastomer nanocomposites. (c) Stretching, bending, twisting, and toughness of the graphite nanoflake/nitrile elastomer nanocomposite strain sensors.

The sensor can be attached onto the various sensing locations on human epidermis for reliable monitoring of multi-scale human motions with high sensitivity due to the ease of human epidermis movements. The light weight property of the proposed strain sensor can be illustrated by holding the device on a plant leaf as shown in Fig. 2a. The leaf exhibited almost negligible deformation, indicating the captivating lightweight property of the graphite nanoflake/nitrile elastomer nanocomposite for its utilization in flexible and wearable electronic systems. The carbon nanomaterials interact with the elastic polymers through van der Waals forces and unzipping of the conductive network occurs during the stretching-releasing cycles in order to dissipate energy and transfer stress, which substantially enhances the mechanical strength, anti-fatigue and recovery properties of the graphite nanoflake/nitrile elastomer nanocomposites.[38] As illustrated in Fig. 2b, graphite nanoflake/nitrile elastomer composites could be designed with ease in different shapes, such as heart, triangle, and star shapes in order to suit different applications. Moreover, the nanocomposites could tolerate significant stretching after holding as well as bending and twisting, indicating the prominent flexibility of nanocomposites (Fig. 2c). When the mechanical deformation was removed after dynamic stretching-releasing cycles, the graphite nanoflake/nitrile elastomer nanocomposites could readily recover to their original dimensions, demonstrating prominent anti-fatigue characteristics and recovery properties. Furthermore, the graphite nanoflake/nitrile elastomer nanocomposites exhibited excellent puncture resistance, which is superior to recently reported flexible electronic devices.[38] These demonstrations indicate that the graphite nanoflake/nitrile elastomer nanocomposites could be employed as stretchable and wearable strain sensors for the monitoring of human activities. Such wearable, and stretchable strain sensors can be directly mounted onto irregular and highly deformable surfaces for continuous strain monitoring with negligible delamination or slippage from the complicated target objects.

The strain sensing properties of the graphite nanoflake/nitrile elastomer strain sensors were studied. The prominent network cracks-assisted electromechanical sensing mechanism for the generation and propagation of electron conduction in graphite nanoflake pathways under tensile strains is schematically illustrated in Fig. 4b. The wearable strain sensor owes its stretching ability to the highly elastic and stretchy property of the nitrile rubber and the graphite nanoflakes are responsible for the strong piezoresistivity. As it can be clearly noticed, under the un-strained condition of the sensor, the graphite nanoflakes are densely packed, with many electron conduction pathways resulting in a highly conductive network. When the electronic device is stretched, the adjacent graphite nanoflakes begin to drift far-away, producing a low areal density. In this scenario, only a small number of graphite nanoflakes hinge together providing lesser pathways for electron conduction, which provide the electrical response as the device is deformed. When the device is stretched further, the adjacent graphite nanoflakes are disconnected with an almost negligible electron conduction pathway, thereby enhancing the electrical resistance enormously. The electromechanical characteristics of the graphite nanoflakes/nitrile rubber nanocomposites were evaluated by stretching the devices and at the same time recording the electrical resistance across the nanocomposite. The relevant electrical resistance variation due to the tensile strains while stretching occurs from the variations in contact resistance due to the rearrangement of the graphite nanoflake networks. As shown in Fig. 3a, the strain sensor exhibits relatively lower strain sensitivity at the initial strain loading, followed by an ultra-fast increment in electrical resistance leading to ultra-large strain sensitivity of the sensor. Moreover, as the strain sensor is of resistive-type with graphite nanoflakes as the active materials, the increment in strain sensitivity also results from the geometrical effects such as reduced film thickness, and decreased length and areal density of graphite nanoflakes.[1,2,39] The electrical resistance variation is relatively lower up to 12% strain, as shown in the inset of Fig. 3a, because the electrically conductive nanomaterials, that is, graphite nanoflakes did not disconnect substantially with the graphite nanoflakes still being close to one another, therefore, the increment in electrical resistance is proportional with the tensile strains, leading to a slight relative resistance variation ($\Delta R/R_0 < 50$).

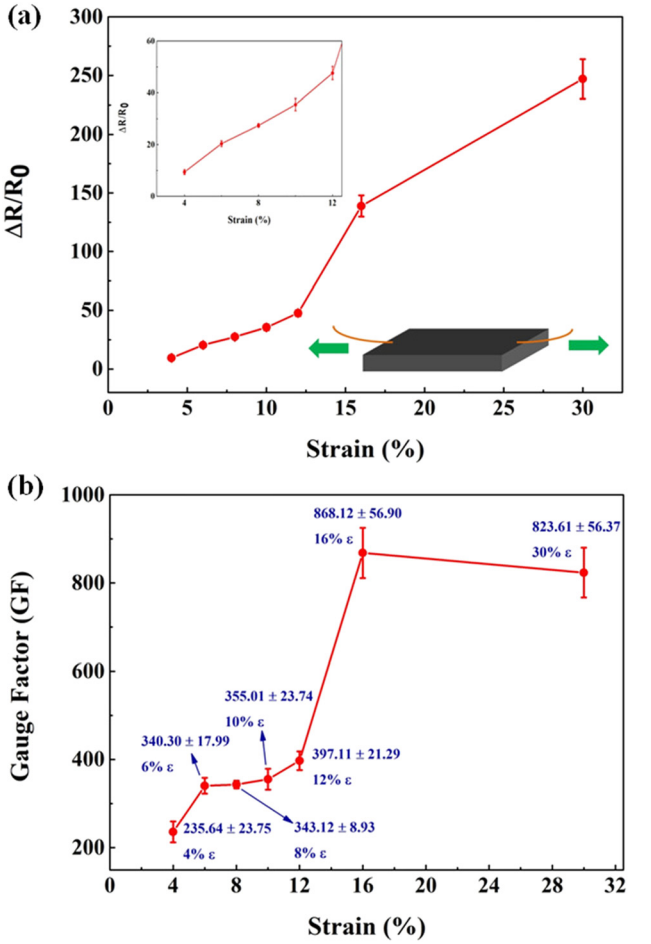

Fig. 3 Strain monitoring performances of graphite nanoflake/nitrile elastomer nanocomposites. (a) Relative resistance variation as a function of the tensile strains for the graphite nanoflake/nitrile elastomer nanocomposite strain sensors. (b) GFs of the graphite nanoflake/nitrile elastomer nanocomposite strain sensors as a function of the tensile strains.

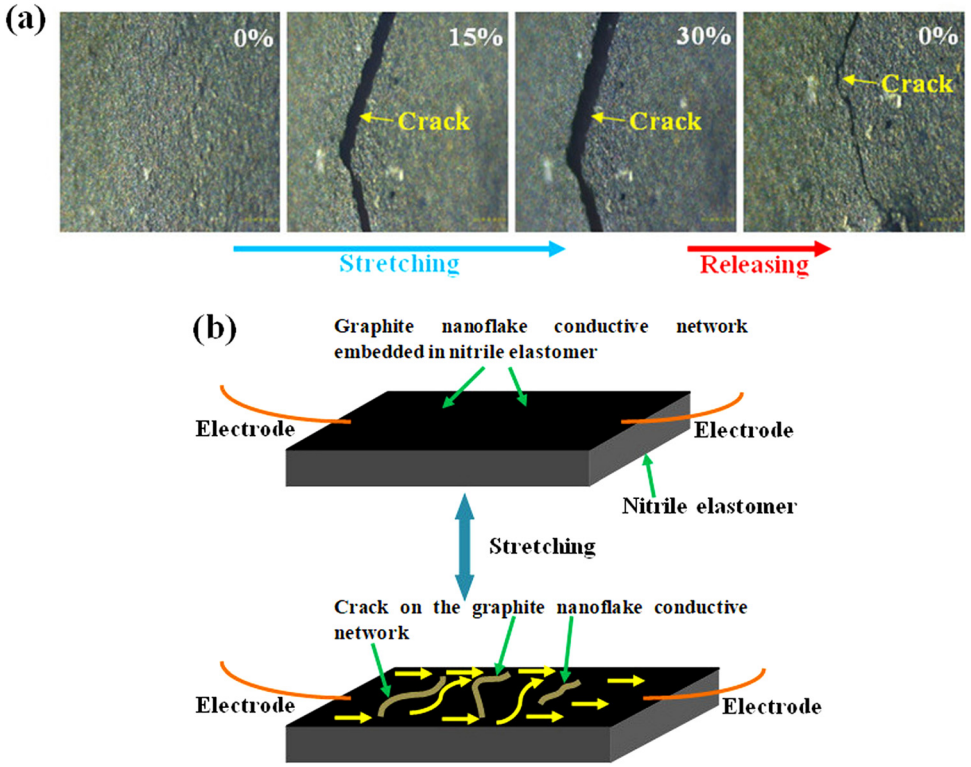

Fig. 4 (a) Top-view optical images illustrating the network-cracks morphology of the graphite nanoflake/nitrile elastomer nanocomposites at tensile strains of 0%, 15%, 30%, and 0%. (b) Schematic evolutions of the network cracks-based structural morphology variation of the graphite nanoflake/nitrile elastomer nanocomposite strain sensor while strain-free and at a stretched state.

As the magnitude of tensile strain increases, the structural cracks are formed in the conductive network and the graphite nanoflakes disconnect substantially, thereby providing fewer electrically conductive pathways and increasing the electrical resistance enormously resulting in ultra-large gauge factors (GFs).

The strain sensitivity of the proposed wearable strain sensor is illustrated in Fig. 3b. Under tensile strains, the graphite nanoflake/nitrile rubber nanocomposite exhibits ultra-large GF values of 823.61 ± 56.37 at 30%, 868.12 ± 56.90 at 16%, 397.11 ± 21.29 at 12%, 355.01 ± 23.74 at 10%, 343.12 ± 8.93 at 8%, 340.30 ± 17.99 at 6%, and 235.64 ± 23.75 at 4% strain, respectively. In previously reported works, the strain sensors based on carbon nanomaterials (*e.g.* graphene reinforced carbon nanotube) and metal nanomaterials (*e.g.* silver nanowire) rarely demonstrated ultra-large strain sensitivity (GF ~ 0.36, and 3.31).[40,41] Moreover, their sensing strain ranges were also low (ε ~ 20%). Therefore, it is worth mentioning that the spray coated graphite nanoflake/nitrile elastomer strain sensors exhibited a high performance with regard to ultra-large strain sensitivity, and a wide strain sensing range simultaneously, which would be beneficial for precise strain monitoring. The strain sensor performance properties are compared with previous studies in Table 1. Based on the above discussion, the shape of the conductive coating layer of the graphite nanoflake/nitrile elastomer composites plays

Table 1 Comparison of GF, stretchability, dynamic durability, response time, and other versatile properties of stretchable strain sensors based on carbonaceous and other active materials

System	Sensing mechanism	Relative resistance variation (%)	GF	Stretchability (%)	Dynamic durability	Response time (ms)	Ref.
Carbon nanotube/ polydimethylsiloxane	Piezoresistive	>300	10	60	>1000 cycles (at 15% strain)	204	42
Reduced graphene oxide nanosheets/nylon-polyurethane fabric	Piezoresistive	>350	18.5	30	>120 cycles (at 3% strain)	—	43
Carbon sponge/ polydimethylsiloxane	Piezoresistive	>2500	130.49	60	>1000 cycles (at 5% strain)	50	44
Silver nanowires/ polydimethylsiloxane	Capacitive	>60	2	30	>1000 cycles (at 10% strain)	—	45
graphite nanoplates/polyurethane	Piezoresistive	>600	20	30	>1000 cycles (at 20% strain)	—	46
graphite nanoflakes/nitrile elastomers	Piezoresistive	>25 000	868.12 ± 56.90	30	>2000 cycles (at 30% strain)	7.5	This work

a prominent role in determining the piezoresistive properties. Moreover, the ultra-high GF through the straight line type shape of conductive layers demonstrates an attractive perspective for emerging wearable and strain sensing applications.

At the deformation free state of the sensor, the neighbouring graphite nanoflakes are overlapped with each other and the porous structural features are embedded within the conductive networks leading to the formation of highly conductive and robust stretchable sensors. At this state, the graphite nanoflakes are interconnected efficiently and highly dense conductive networks are observed as illustrated in Fig. 1c and d through SEM images. The structural pores exhibit a negligible contribution toward the overall initial conductivity of the spray coated stretchable strain sensors. When the structural pores are absent in the conductive networks, tiny mechanical deformation results in the reduction of overlapping area and the disconnection of adjacent graphite nanoflakes occur. For the stretchable sensors with significant pores, the evolution of the porous structures occurs in addition to the disconnection and loss of the overlapped area among adjacent graphite nanoflakes. This feature leads to the enhancement of electrical responses of the sensor and thereby improves the sensitivity or gauge factors (GFs). For large-scale vigorous mechanical deformations, the ruination of graphite nanoflake conductive networks combined with the extensive expansion of structural pores results in the achievement of high performance, specifically in terms of gauge factors (GFs). In addition to the above-mentioned working mechanisms, the electrical responses of the as-fabricated strain sensors are attributed to the generation and propagation of structural cracks of brittle graphite films and the corresponding electrically conductive pathways are schematically illustrated in Fig. 5. At a lower strain range, the strain sensors demonstrated a gentle decrease in the electrical conductivity (Fig. 3a). Even though structural cracks were observed in the graphite nanoflake/nitrile elastomer composite (Fig. 4a), still the cracks were unable to destruct the electrically conductive pathways fully owing to the shorter crack width, resulting in lower strain sensitivity. On the other hand, when the electronic device is deformed further, fewer conductive pathways were observed in the specimen owing to the presence of relatively larger structural cracks, leading to a substantial reduction in the electrical conductivity giving rise to ultra-high gauge factors.

The strain sensing mechanisms of the relative resistance variations of the graphite nanoflake/nitrile rubber elastomers under various mechanical deformations are examined subsequently. The micro-morphologies of the graphite nanoflake/nitrile elastomers under various external strains are analyzed through optical micrographs as shown in Fig. 4a. The strain levels on the graphite nanoflake/nitrile rubber elastomers change from 0% strain to 30% strain during the whole external deformation process. Due to this external deformation, the network cracks are formed and propagate gradually exhibiting crack enlargement as well as rupturing of the electrically

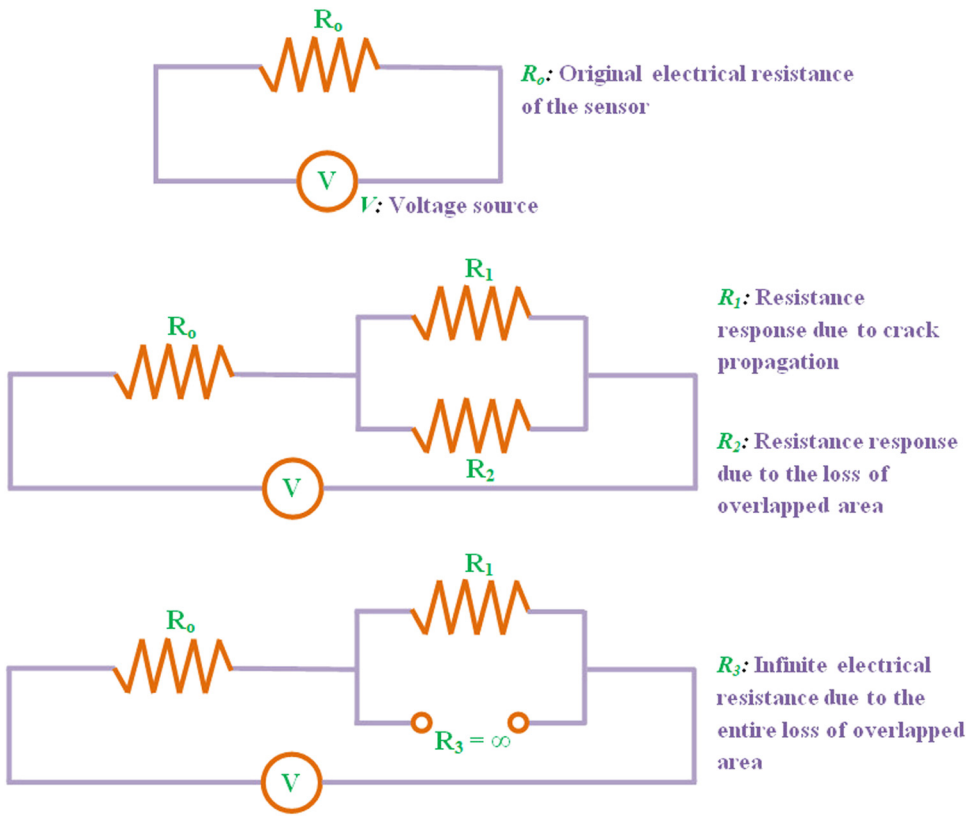

Fig. 5 Schematic illustrating the electrical resistance networks of the graphite nanoflake/nitrile elastomer nanocomposite strain sensors at a strain-free state, small-scale tensile strain, and at a large-scale tensile strain, respectively.

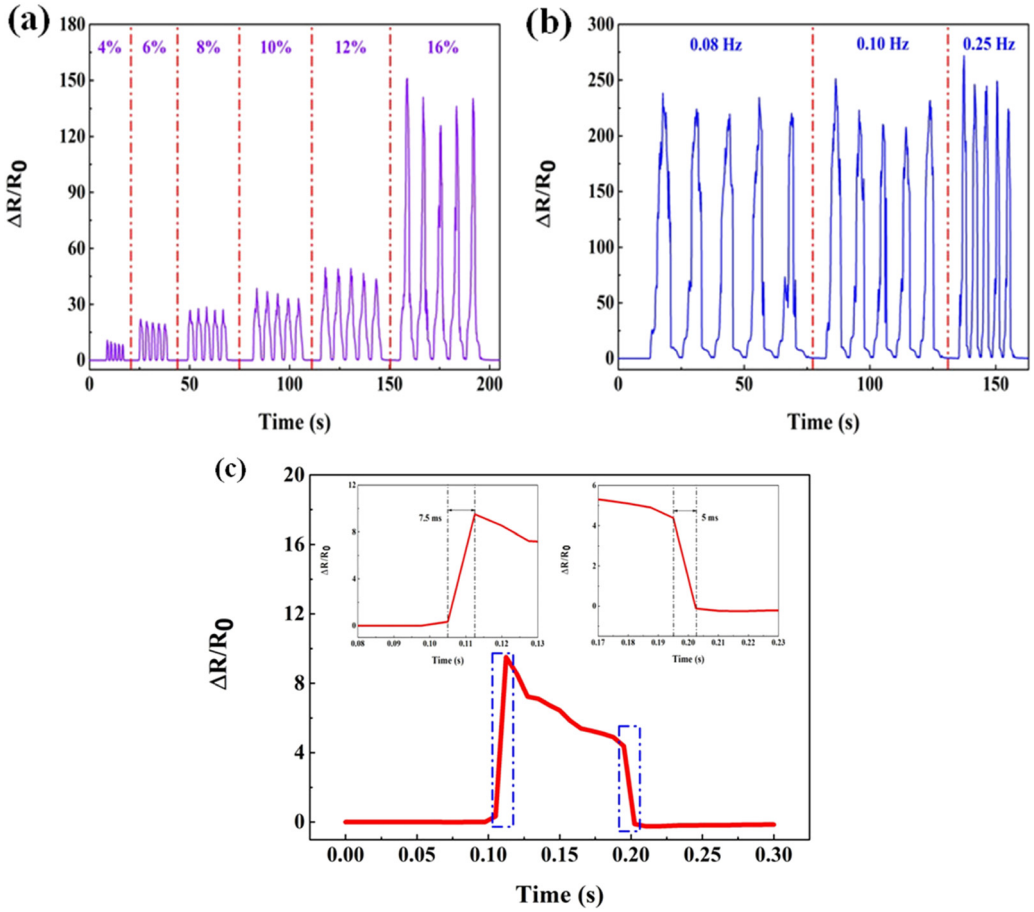

Fig. 6 (a) The relative resistance variation of the graphite nanoflake/nitrile elastomer nanocomposite strain sensors to dynamic stretching-releasing cyclic tensile strains. (b) The relative resistance variation of the graphite nanoflake/nitrile elastomer nanocomposite strain sensors with various stretching frequencies (0.08, 0.10, and 0.25 Hz) under a large-scale mechanical deformation of 30% strain. (c) The response and recovery time of the graphite nanoflake/nitrile elastomer nanocomposite strain sensors under a mechanical deformation of 5% strain.

conductive pathways resulting in ultrahigh gauge factors or ultra-large strain sensitivity (Fig. 3b), which can be a benefit for monitoring small-scale human healthcare signals such as blood flow pulse waveforms, larynx muscle motions and vibration of the vocal cords, and human facial microexpressions. Moreover, Fig. 4a shows the process of releasing the external strains from a strain level of 30% to 0%. It is worth mentioning that the network cracks regained their original states, which specifically explains the prominent reversible characteristics (Fig. 6a and b) observed in these wearable devices. The above discussed strain sensing mechanisms of the graphite nanoflake/nitrile elastomer nanocomposites are shown in Fig. 4b and the respective electrical resistance networks are schematically shown in Fig. 5.

To further evaluate the electromechanical characterization data of the straight-line type graphite nanoflake/nitrile elastomer composite strain sensors, dynamic stretch-release cycles under 4%, 6%, 8%, 10%, 12% and 16% strain range and 30% strain under 0.08, 0.10, and 0.25 Hz stretching frequencies were subjected onto them (Fig. 6a and b). The relative resistance variations for the sensors were stable and reliable at the respective strain ranges. Furthermore, during different stretching frequencies, the shape of the electrical response conforms well, *i.e.*, the strain sensor performance is not destructed with the enhancement of stretching frequency, implying that the electrical response is independent of tensile frequency in the range of 0.08–0.25 Hz. The above discussed results would be beneficial for detecting as well as monitoring of high-speed and energetic human bodily motions.

Next, the response and recovery times of straight-line type graphite nanoflake/nitrile elastomer composite strain sensors were estimated under quasi-instantaneous small-strain ($\varepsilon \sim 5\%$) conditions as illustrated in Fig. 6c. The electronic devices were stretched at a high strain rate of 600 mm min^{-1}, the electrical responses were prompt with a super-fast response and recovery time of 7.5, and 5 ms, respectively. The inset of Fig. 6c depicts the relative resistance variation *versus* time plot of the dynamic stretch-release cycle with a strain of 5% for the estimation of response and recovery time. The rapid response/recovery time of the proposed strain sensor inspires confidence that the electronic device is suitable for super-fast monitoring of human bodily motions and healthcare related vital signs. To the best of my knowledge, the strain sensor response/recovery times obtained in this work are fascinating as compared to the recently reported state of the art wearable strain sensors as illustrated in Table 2.

Table 2 Summary of the performance characteristics in terms of the response and recovery times of recently reported state of the art stretchable strain sensors

System	Sensing mechanism	Manufacturing method	Response time (ms)	Recovery time (ms)	Ref.
Vertically aligned carbon nanotube/ poly(dimethylsiloxane)	Piezoresistive	Chemical vapor deposition	12	19	39
Carbon nanotube/thermoplastic polyurethane	Piezoresistive	Compression molding and salt leaching	180	180	47
Aramid nanofiber/polyvinyl alcohol	Piezoresistive	Oxidative polymerization	214	252	48
Reduced graphene oxide-deionized water/ecoflex	Piezoresistive	Modified Hummers' method	60.3	60.4	49
Silver nanofibers/ionic hydrogels	Piezocapacitive	Drop coating	130	320	50
Carbon nanotube/ecoflex	Optical	Spray coating	<50	—	51
Wrinkled chitosan-multiwall carbon nanotube/ poly(dimethylsiloxane)	Piezoresistive	Spray coating	400	—	52
graphite nanoflakes/nitrile elastomers	Piezoresistive	Spray coating	7.5	5	This work

Furthermore, the straight line type graphite nanoflake/nitrile elastomer composite strain sensor exhibited reliable strain monitoring characteristics with a stable electrical response (after a pre-stretching strain of 10% for 5 stretch-release cycles) (Fig. 6). The pre-stretching process of the graphite nanoflake/nitrile elastomer composite strain sensor before evaluating its electromechanical properties demonstrates many advantages such as enlargement of the strain sensitivity in the whole strain range, which leads to the improvement of strain monitoring of the electronic device. Moreover, the stability of the acquired signals is also improved with a prominent signal to noise ratio owing to the effective transfer of mechanical deformation onto the electronic device. After that, the long-term stability of the straight line type graphite nanoflake/nitrile elastomer composite strain sensor was investigated as

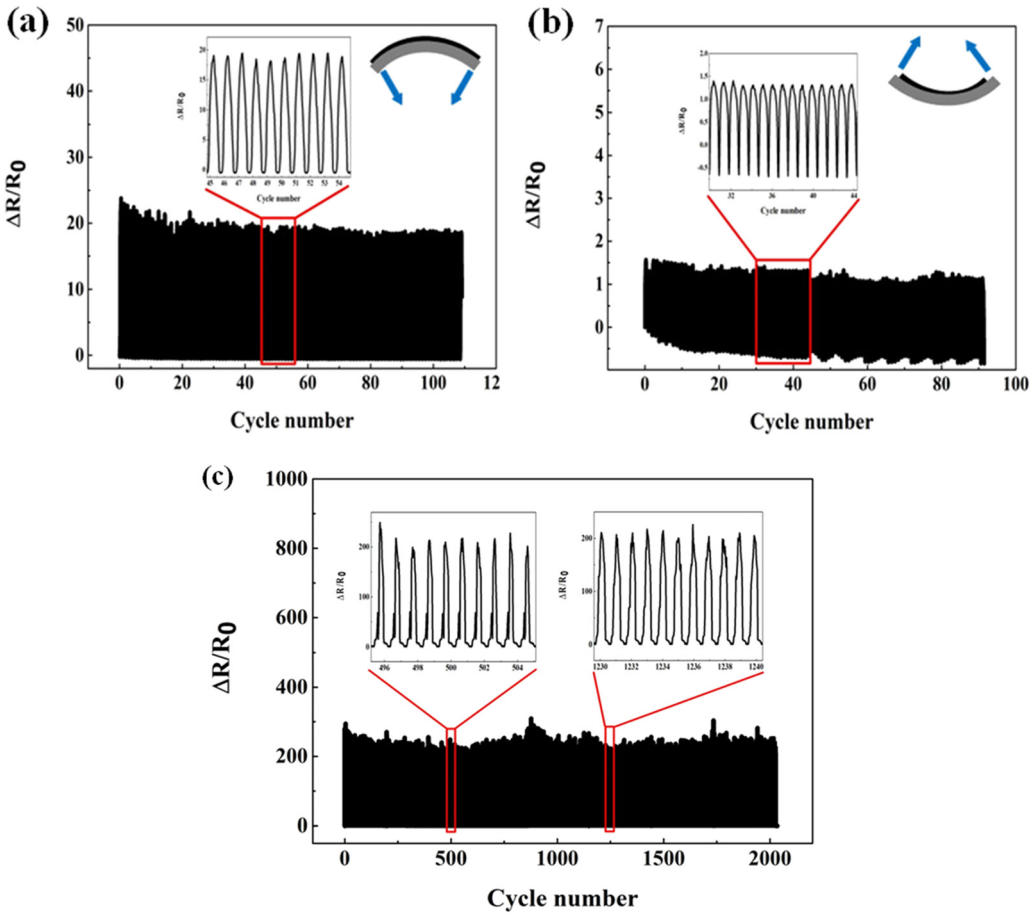

Fig. 7 Relative resistance variation of the graphite nanoflake/nitrile elastomer nanocomposite strain sensors under various dynamic cyclic strains. Relative resistance variation for tensile bending at a frequency of 0.25 Hz for more than 100 cycles (a) or compression bending at a frequency of 0.25 Hz for more than 80 cycles (b) at a bending radius of 4 mm. (c) Durability test of the graphite nanoflake/nitrile elastomer nanocomposite strain sensors at a frequency of 0.25 Hz under an extensive mechanical deformation of 30% strain for more than 2000 stretch-release cycles.

shown in Fig. 7c. The strain sensors demonstrated a reproducible electrical response with retention of their high sensitivity after each stretch-release cycle under a large-scale dynamic strain of 30% for more than 2000 cycles, implying that the electronic devices exhibit excellent reliability and durability, which would be beneficial for practical applications, for example, while monitoring the large-strain human activities (bending process of a finger, wrist, elbow, and knee joint motions). In a previous work, Tian *et al.* presented an Ag nanodendrite/nitrile elastomer composite strain sensor which demonstrated an un-reliable performance for around 300 stretch-release cycles under a strain range of 30% with significant drifting in its electrical response.[23] In contrast, the graphite nanoflake/nitrile elastomer composite strain sensors reported in this work demonstrate a stable durability and reproducibility for more than 2000 stretching-releasing cycles under a large-scale strain of 30%.

The relative resistance variations of the straight line type graphite nanoflake/nitrile elastomer composite strain sensor for five stretch-release cycles at 4%, 6%, 8%, 10%, 12%, and 16% strain ranges, respectively, are illustrated in Fig. 6a. It can be clearly observed that the stretchable strain sensor demonstrates a prominent recovery performance while the external strain is reversed with negligible hysteretic characteristics. In a recently reported work based on a silver nanodendrite/nitrile elastomer composite strain sensor,[23] the hysteresis characteristics increase during the increment of external strain amplitude. This strain responsive behaviour was attributed to the Mullins effect of nitrile elastomers, which exhibits irreversible and quasi-instantaneous softening while loading-unloading external strains. In contrast, the wearable and stretchable strain sensors presented in this research exhibit excellent strain sensing performances.

In general, a wearable strain sensor with a large strain sensitivity normally exhibits a recognition ability for face expressions, blood flow pulse,[53] and breathing monitoring. In contrast, a strain sensor with a broad strain range can typically be utilized for large-scale strain monitoring like human articular joint motions.[54] On the other hand, the graphite nanoflake/nitrile elastomer composite strain sensors presented in this research can not only monitor large-scale mechanical deformations, but also demonstrate the ability of detecting tiny mechanical stimulations promptly.

Apart from monitoring tensile stretching strains, the electrical responses of the straight line type graphite nanoflake/

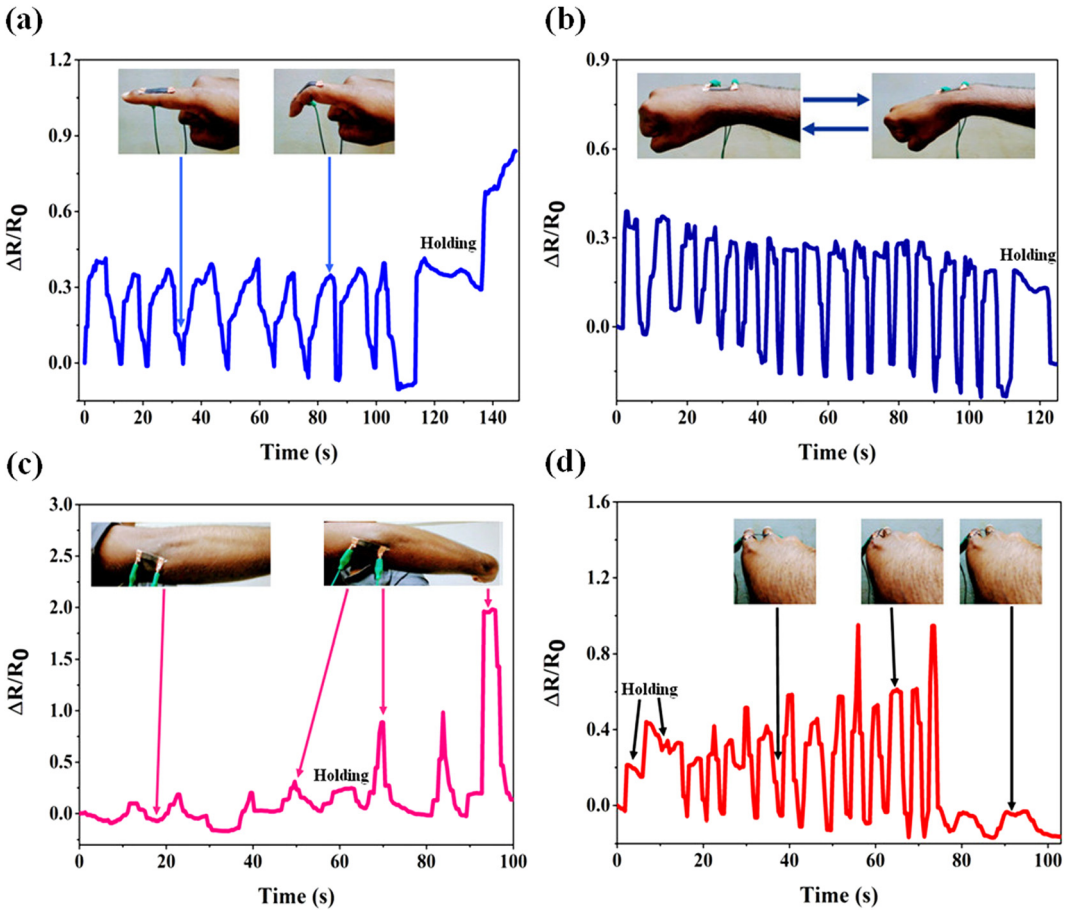

Fig. 8 Monitoring of large-scale human motions by the graphite nanoflake/nitrile rubber nanocomposite strain sensor. The relative resistance variation of the strain sensor to (a) bending and holding process of a finger, (b) wrist bending, (c) bending and holding of an elbow joint, and (d) closing process of the fingers. Insets: Photographs of the graphite nanoflake/nitrile rubber nanocomposite strain sensor mounted onto the index finger knuckles, wrist, elbow joint, and in between the fingers with corresponding motions.

nitrile elastomer composite strain sensor during the application of tensile and compressive bending strains was also evaluated. The relative resistance variation during the application of bending strains is shown in Fig. 7a and b. The electronic sensor was fixed firmly on top of a steel plate using cyanoacrylate adhesive. The stepper was propelled on one end of the sensor with another end fixed for dynamic cyclic bending investigation. The strain sensor exhibited a sharp increase in its electrical response during outward or tensile bending and increased minutely with inward or compressive bending. For instance, the electrical response is $\sim$20 for tensile bending and during compressive bending, it is $\sim$1.5 under the same bending radius of 4 mm. The tensile bending leads to the widening of gaps in between the islands, which results in the enhancement of electrical resistance. In contrast, during compressive bending, the alteration of the crack morphology was not significant and therefore, the electrical response increased tardily. Furthermore, the graphite nanoflake/nitrile elastomer composite strain sensor demonstrates a reproducible electrical response under both tensile and compressive bending strains.

Human motion monitoring

Motivated by the ultrahigh gauge factors of the graphite nanoflake/nitrile elastomer composite based wearable strain sensors, sensing demonstrations were conducted with regard to the practical wearable sensing applications utilizing these devices for full-range human motion and posture monitoring including tiny mechanical stimulations (eye blinking, frowning, and larynx muscle movements) as well as large-strain mechanical deformations (bending process of a finger, closing-opening of fingers, wrist, and elbow joint bending/recovering movements).

In order to demonstrate the applicability of these electronic devices for large-strain human motion monitoring, the wearable sensors were laminated onto the human articular joints with the assistance of double-sided tape. As shown in Fig. 8, it

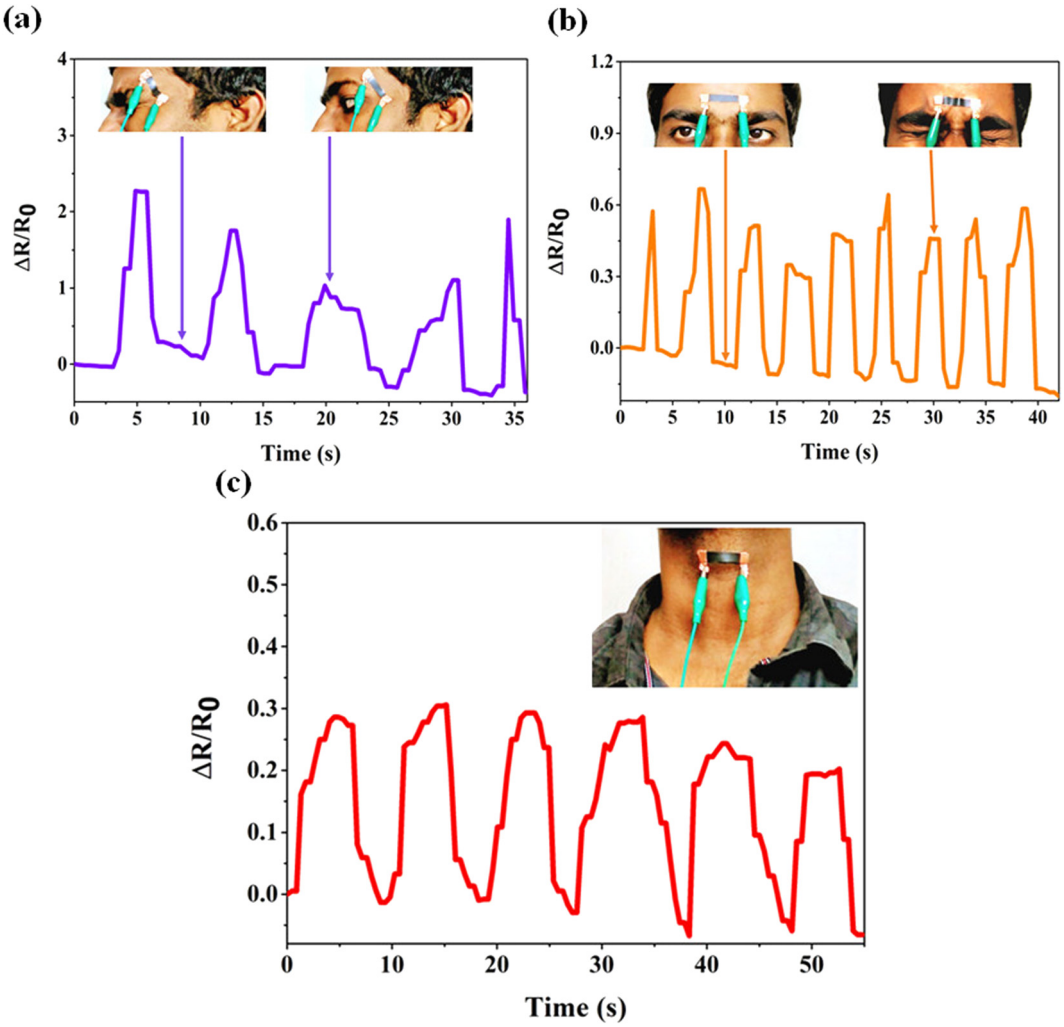

Fig. 9 Monitoring of small-scale human motions by the graphite nanoflake/nitrile rubber nanocomposite strain sensor. The relative resistance variation of the strain sensor to (a) blinking of an eye, (b) frowning, and (c) vibration of the vocal cords while phonating different words. Insets: Photographs of the graphite nanoflake/nitrile rubber nanocomposite strain sensor mounted onto the epidermal canthus region, forehead, and larynx with respective movements.

can be clearly observed that the wearable strain sensor can monitor in real-time, finger, wrist, and elbow bending (with different angles) and holding movements in a prompt, reliable, and repeatable manner. To further demonstrate the utilization of the graphite nanoflake/nitrile elastomer composite strain sensors for wearable sensing applications, posture monitoring of the two fingers were demonstrated. As shown in Fig. 8d, the wearable device was laminated in between the two fingers for monitoring their posture during closing-opening movement of fingers in both tension bending as well as compression bending. The wearable strain sensor exhibited a rapid and stable response in a step-wise fashion with effective synchronization with the applied mechanical strain. These results demonstrate that the wearable strain sensors can be employed as motion sensors for healthcare and biomedical engineering, entertainment technology, and virtual reality. The body movements are critical for posture-driven gaming, physiotherapy, home-rehabilitation, and medical training.[2]

Apart from the large-strain human motion monitoring discussed above, the detection of tiny mechanical stimulations such as larynx muscle activity while drinking water and speaking, and facial expressions while frowning, and blinking of an eye can be reliably carried out utilizing the graphite nanoflake/nitrile elastomer composite strain sensor. For these sensing demonstrations, the wearable strain sensors were laminated onto the epidermis over the throat, forehead, and canthus of a volunteer.

As shown in Fig. 9c, the muscle tissue movements while drinking water and speaking can be monitored utilizing the graphite nanoflake/nitrile elastomer composite strain sensor by achieving conformal and intimate lamination with the volunteer's throat using strong double-side tape. Moreover, the wearable strain sensor was employed for face expression recognition by detecting the facial muscle motions during eye blinking and frowning, as shown in Fig. 9a and b. These results imply that the graphite nanoflake/nitrile elastomer composite strain sensor could differentiate various emotional states of humans with high sensitivity and stability. Hence, the graphite nanoflake/nitrile elastomer composite strain sensor could be utilized for real-time monitoring of both tiny mechanical stimulations (larynx movements and facial expressions) and large-strain human motion monitoring (bending process of a finger, close-open posture of fingers, wrist, and elbow joint movements).

Conclusions

In summary, this research presented stretchable, wearable and skin-mountable strain sensors comprising of graphite nanoflakes embedded onto highly elastic and epidermis-like nitrile elastomers. Through the strain induced network cracks, the strain sensors demonstrate an ultra-large strain sensitivity (868.12 ± 56.90), which is substantially enhanced by more than 400 times relative to that of traditional metallic foil-based strain gauge sensors (GF = 2). Moreover, the graphite nanoflake/nitrile elastomer nanocomposite-based strain sensor exhibits a wide sensing range of up to 30%, ultra-fast response and recovery speeds (7.5 ms, and 5 ms, respectively), low creep, and excellent durability (more than 2000 stretching-releasing cycles under an extensive deformation of 30% strain). Through sensing demonstrations with regard to wearable monitoring applications, the graphite nanoflake/nitrile elastomer nanocomposites are envisioned as promising components for smart wearable electronics, including but not limited to human motion/health monitoring (disease diagnosis, voice rehabilitation, biophysical parameter monitoring, physiology, and kinesiology applications), soft robotics and neuromechanics, and entertainment technology (virtual reality, posture driven gaming, and teleoperated robotics). It is believed that the technology based on graphite nanoflakes/nitrile elastomer nanocomposites and a scalable fabricating strategy to construct ultrasensitive and cost-effective stretchable strain sensors may further result in the improvement of sensitivity of other wearable monitoring devices.

Conflicts of interest

There are no conflicts to declare.

References

1 M. Amjadi, K.-U. Kyung, I. Park and M. Sitti, *Adv. Funct. Mater.*, 2016, **26**, 1678–1698.
2 H. Souri, H. Banerjee, A. Jusufi, N. Radacsi, A. A. Stokes, I. Park, M. Sitti and M. Amjadi, *Adv. Intell. Syst.*, 2020, **2**, 2000039.
3 W. Gao, H. Ota, D. Kiriya, K. Takei and A. Javey, *Acc. Chem. Res.*, 2019, **52**(3), 523–533.
4 W. Zhai, C. Wang, S. Wang, J. Li, Y. Zhao, P. Zhan, K. Dai, G. Zheng, C. Liu and C. Shen, *J. Mater. Chem.*, 2021, **9**, 7238–7247.
5 Y. Song, J. Min and W. Gao, *ACS Nano*, 2019, **13**(11), 12280–12286.
6 J. Wang, C. Lu and K. Zhang, *Energy Environ. Mater.*, 2019, **3**, 80–100.
7 J. Wu, Z. Wu, X. Lu, S. Han, B.-R. Yang, X. Gui, K. Tao, J. Miao and C. Liu, *ACS Appl. Mater. Interfaces*, 2019, **11**(9), 9405–9414.
8 N. Qaiser, F. Al-Modaf, S. M. Khan, S. F. Shaikh, N. El-Atab and M. M. Hussain, *Adv. Funct. Mater.*, 2021, **31**, 2103375.
9 T. Q. Trung and N.-E. Lee, *Adv. Mater.*, 2016, **28**, 4338–4372.
10 S. Lim, D. Son, J. Kim, Y. B. Lee, J.-K. Song, S. Choi, D. J. Lee, J. H. Kim, M. Lee, T. Hyeon and D.-H. Kim, *Adv. Funct. Mater.*, 2015, **25**, 375–383.
11 E. Roh, B.-U. Hwang, D. Kim, B.-Y. Kim and N.-E. Lee, *ACS Nano*, 2015, **9**(6), 6252–6261.
12 M. Zhu, Q. Shi, T. He, Z. Yi, Y. Ma, B. Yang, T. Chen and C. Lee, *ACS Nano*, 2019, **13**(2), 1940–1952.
13 O. A. Araromi, M. A. Graule and K. L. Dorsey, *et al.*, *Nature*, 2020, **587**, 219–224.

14 Z. Zhan, R. Lin, V.-T. Tran, J. An, Y. Wei, H. Du, T. Tran and W. Lu, *ACS Appl. Mater. Interfaces*, 2017, **9**(43), 37921–37928.
15 H. Souri and D. Bhattacharyya, *J. Mater. Chem. C*, 2018, **6**, 10524–10531.
16 V. Sankar, A. Nambi, V. N. Bhat, D. Sethy, K. Balasubramaniam, S. Das, M. Guha and R. Sundara, *ACS Omega*, 2020, **5**(22), 12682–12691.
17 O. Atalay, A. Atalay, J. Gafford, H. Wang, R. Wood and C. Walsh, *Adv. Mater. Technol.*, 2017, **2**, 1700081.
18 F. Mo, Y. Huang, Q. Li, Z. Wang, R. Jiang, W. Gai and C. Zhi, *Adv. Funct. Mater.*, 2021, **31**, 2010830.
19 M. Xu, X. Li, C. Jin, Z. He, X. Zhang and Q. Zhang, *J. Mater. Chem. C*, 2020, **8**, 1466–1474.
20 S.-H. Park, H. B. Lee, S. M. Yeon, J. Park and N. K. Lee, *ACS Appl. Mater. Interfaces*, 2016, **8**(37), 24773–24781.
21 R. Fu, T. Warnakula, Q. Shi, L. W. Yap, D. Dong, Y. Liu, M. Premaratne and W. Cheng, *Nanoscale Horiz.*, 2020, **5**(11), 1515–1523.
22 X. Liao, Z. Zhang, Z. Kang, F. Gao, Q. Liao and Y. Zhang, *Mater. Horiz.*, 2017, **4**, 502–510.
23 B. Tian, W. Yao, P. Zeng, X. Li, H. Wang, L. Liu, Y. Feng, C. Luo and W. Wu, *J. Mater. Chem. C*, 2019, **7**(4), 809–818.
24 J. Heikenfeld, A. Jajack, J. Rogers, P. Gutruf, L. Tian, T. Pan, R. Li, M. Khine, J. Kim, J. Wang and J. Kim, *Lab Chip*, 2018, **18**, 217–248.
25 X. Liao, Z. Zhang, Q. Liang, Q. Liao and Y. Zhang, *ACS Appl. Mater. Interfaces*, 2017, **9**(4), 4151–4158.
26 H. Li, J. W. Chen, X. H. Chang, Y. Q. Xu, G. Y. Zhao, Y. T. Zhu and Y. J. Li, *J. Mater. Chem. A*, 2021, **9**, 1795–1802.
27 R. Iglio, S. Mariani, V. Robbiano, L. Strambini and G. Barillaro, *ACS Appl. Mater. Interfaces*, 2018, **10**, 13877–13885.
28 Q. Liu, J. Chen, Y. Li and G. Shi, *ACS Nano*, 2016, **10**(8), 7901–7906.
29 Y.-F. Wang, T. Sekine, Y. Takeda, J. Hong, A. Yoshida, H. Matsui, D. Kumaki, T. Nishikawa, T. Shiba, T. Sunaga and S. Tokito, *ACS Appl. Mater. Interfaces*, 2020, **12**(31), 35282–35290.
30 S. Wang, P. Xiao, Y. Liang, J. Zhang, Y. Huang, S. Wu, S.-W. Kuo and T. Chen, *J. Mater. Chem. C*, 2018, **6**, 5140–5147.
31 H. Yang, X. Xiao, Z. Li, K. Li, N. Cheng, S. Li, J. H. Low, L. Jing, X. Fu, S. Achavananthadith, F. Low, Q. Wang, P.-L. Yeh, H. Ren, J. S. Ho, C.-H. Yeow and P.-Y. Chen, *ACS Nano*, 2020, **14**(9), 11860–11875.
32 S.-J. Park, J. Kim, M. Chu and M. Khine, *Adv. Mater. Technol.*, 2016, **1**, 1600053.
33 Q. Li, R. Yin, D. Zhang, H. Liu, X. Chen, Y. Zheng, Z. Guo, C. Liu and C. Shen, *J. Mater. Chem. A*, 2020, **8**, 21131–21141.
34 Z. Liu, Y. Zheng, L. Jin, K. Chen, H. Zhai, Q. Huang, Z. Chen, Y. Yi, M. Umar, L. Xu, G. Li, Q. Song, P. Yue, Y. Li and Z. Zheng, *Adv. Funct. Mater.*, 2021, **31**, 2007622.
35 S. Pan, Z. Liu, M. Wang, Y. Jiang, Y. Luo, C. Wan, D. Qi, C. Wang, X. Ge and X. Chen, *Adv. Mater.*, 2019, 1903130.
36 S. Niu, N. Matsuhisa and L. Beker, *et al.*, *Nat. Electron.*, 2019, **2**, 361–368.
37 S. Park, H. Choi, Y. Cho, J. Jeong, J. Sun, S. Cha, M. Choi, J. Bae and J.-J. Park, *ACS Appl. Mater. Interfaces*, 2021, **13**(19), 22926–22934.
38 S. Xia, S. Song and G. Gao, *Chem. Eng. J.*, 2018, **354**, 817–824.
39 S. J. Paul, I. Elizabeth and B. K. Gupta, *ACS Appl. Mater. Interfaces*, 2021, **13**(7), 8871–8879.
40 J. Shi, X. Li, H. Cheng, Z. Liu, L. Zhao, T. Yang, Z. Dai, Z. Cheng, E. Shi, L. Yang, Z. Zhang, A. Cao, H. Zhu and Y. Fang, *Adv. Funct. Mater.*, 2016, **26**, 2078–2084.
41 J. Eom, J.-S. Heo, M. Kim, J. H. Lee, S. K. Park and Y.-H. Kim, *RSC Adv.*, 2017, **7**, 53373–53378.
42 M. Nankali, N. M. Nouri, M. Navidbakhsh, N. Geran Malek, M. A. Amindehghan, A. Montazeri Shahtoori, M. Karimi and M. Amjadi, *J. Mater. Chem. C*, 2020, **8**, 6185–6195.
43 G. Cai, M. Yang, Z. Xu, J. Liu, B. Tang and X. Wang, *Chem. Eng. J.*, 2017, **325**, 396–403.
44 He Gong, C. Cai, H. Gu, Q. Jiang, D. Zhang and Z. Cheng, *RSC Adv.*, 2021, **11**(7), 4186–4193.
45 S.-R. Kim, J.-H. Kim and J.-W. Park, *ACS Appl. Mater. Interfaces*, 2017, **9**(31), 26407–26416.
46 J. Wu, Z. Ma, Z. Hao, J. T. Zhang, P. Sun, M. Zhang, Y. Liu, Y. Cheng, Y. Li, B. Zhong, T. Zhang, L. Xia, W. Yao, X. Huang, H. Wang, H. Liu, F. Yan, C. E. Hsu and G. Xing, *ACS Appl. Nano Mater.*, 2019, **2**(2), 750–759.
47 C.-G. Zhou, W.-J. Sun, L.-C. Jia, L. Xu, K. Dai, D.-X. Yan and Z.-M. Li, *ACS Appl. Mater. Interfaces*, 2019, **11**(40), 37094–37102.
48 J. Wang, Y. Lin, A. Mohamed, Q. Jib and H. Jia, *J. Mater. Chem. C*, 2021, **9**, 575–583.
49 M. Xu, J. Qi, F. Li and Y. Zhang, *Nanoscale*, 2018, **10**, 5264–5271.
50 H. Xu, Y. Lv, D. Qiu, Y. Zhou, H. Zeng and Y. Chu, *Nanoscale*, 2019, **11**, 1570–1578.
51 J. Gu, D. Kwon, J. Ahn and I. Park, *ACS Appl. Mater. Interfaces*, 2020, **12**(9), 10908–10917.
52 B. Zhang, W. Wang, D. Zhang, T. Li, H. Zhang, C. Du, W. Zhaoa and Y. Yanga, *J. Mater. Chem. C*, 2021, **9**, 14848–14857.
53 T. Yang, X. Jiang, Y. Zhong, X. Zhao, S. Lin, J. Li, X. Li, J. Xu, Z. Li and H. Zhu, *ACS Sens.*, 2017, **2**(7), 967–974.
54 Y. Zheng, Y. Li, K. Dai, Y. Wang, G. Zheng and C. Liu, *et al.*, *Compos. Sci. Technol.*, 2018, **156**, 276–286.
55 Y. Bu, T. Shen, W. Yang, S. Yang, Y. Zhao, H. Liu, Y. Zheng, C. Liu and C. Shen, *Sci. Bull.*, 2021, **66**(18), 1849–1857.
56 H. Liu, Q. Li, Y. Bu, N. Zhang, C. Wang, C. Pan, L. Mi, Z. Guo, C. Liu and C. Shen, *Nano Energy*, 2019, **66**, 104143.
57 X. Chang, L. Chen and J. Chen, *et al.*, *Adv. Compos. Hybrid Mater.*, 2021, **4**, 435–450.
58 M. Fan, L. Wu and Y. Hu, *et al.*, *Adv. Compos. Hybrid Mater.*, 2021, **4**, 1039–1047.
59 M. Hu, Y. Gao and Y. Jiang, *et al.*, *Adv. Compos. Hybrid Mater.*, 2021, **4**, 514–520.
60 K. K. Kim, S. Hong, H. M. Cho, J. Lee, Y. D. Suh, J. Ham and S. H. Ko, *Nano Lett.*, 2015, **15**(8), 5240–5247.
61 L. Wang, T. Xu, C. Fan and X. Zhang, *iScience*, 2021, **24**(1), 102028.
62 K. K. Kim, I. Ha and M. Kim, *et al.*, *Nat. Commun.*, 2020, **11**, 2149.
63 R. Madhavan, *J. Mater. Sci.: Mater. Electron.*, 2022, **33**, 3465–3484.
64 R. Madhavan, *Macromol. Mater. Eng.*, 2022, **307**, 2200034.
65 R. Madhavan, *New J. Chem.*, 2022, **46**, 17596–17609.